Preparation of Manganese Dioxide/Polypyrrole Composite by W/O Miniemulsion and Its Electrochemical Performance

Zhiwei Liu[*], *Fangnan Liang, Ning Zhang, Youzhi Liu*

Shanxi Province Key Laboratory of Higee-Oriented Chemical Engineering, North University of China, No. 3, Xueyuan Road, Jiancaoping District, Taiyuan 030051, China
[*]E-mail: lzwww6723487@126.com

A new and convenient synthetic route of W/O miniemulsion technology was used to prepare manganese dioxide/polypyrrole (MnO_2/PPy) composites. The structures and morphologies were characterized by Fourier transform infrared spectroscopy (FTIR), X-ray diffraction (XRD), high resolution transmission electron microscope (HRTEM) and thermogravimetric analysis (TGA). The results indicated that the MnO_2/PPy composite was spheroid and had average particle size of ~200 nm. The relationship between stability of the miniemulsion and the hydrophilic-lipophilic balance (HLB) was firstly evaluated. Moreover, the effects of HLB, $KMnO_4$ amount and reaction time on electrochemical properties of MnO_2/PPy composites were studied by cyclic voltammetry (CV), galvanostatic charge-discharge (GCD), electrochemical impedance spectroscopy (EIS). It was found that the as-synthesized MnO_2/PPy composites exhibited specific capacitance (SC) of 288.7 F g^{-1} at a current density (c.d.) of 0.5 A g^{-1}. The SC was still retained 91.3% after 1000 cycles at 1 A g^{-1}. Therefore, this research proposed a W/O miniemulsion method for preparing the MnO_2/PPy composites with well electrochemical properties.

1. INTRODUCTION

Energy storage in electrical double layer capacitors (EDLC) is caused by embedding/removing the surface ion at the electrode/electrolyte interfaces, while a pseudo-capacitor is mainly based on the surface Faradic reactions [1, 2]. Generally, the pseudo-capacitive materials include transition metal oxides and conducting polymers. Among these optional materials, manganese dioxide (MnO_2) has drawn widespread attention as a promising electrode material, which is inexpensive, natural abundance and environmentally friendly. However, its poor electrical conductivity (10^{-5}-10^{-6} S cm^{-1}) restricts the applications [3]. Conducting polymers show both good electrical conductivity and high reversible

pseudo-capacitance, which can not only enhance the electrochemical utilization of MnO_2 but also make a considerable benefits for the entire capacitance of the composites [4]. Therefore, more and more researchers focus on the composite electrode materials for compensation the drawbacks of the single electrode materials [5-8]. MnO_2/PPy composites have been commonly used as composite electrode materials in pseudo-capacitances owing to their outstanding electrochemical properties [9-13].

The MnO_2/PPy composites have attracted more and more interest due to the cooperative action between MnO_2 and PPy. The MnO_2 in composites can keep the PPy chains stable, while the PPy strengthen the conductivity of MnO_2 and block it from solubilizing into the solution in turn [14]. Consequently, the electrochemical properties of composite material electrodes are higher than the single material electrodes. To date, various techniques such as in-situ redox deposition [15-17], electrodeposition [18, 19], electrostatic interaction assembly [20] and chemical co-precipitation [21] have been developed to prepare MnO_2/PPy composites. For in-situ redox deposition technique, the loading capacity of MnO_2 is greatly restricted since over oxidation will damage the π-conjugated construction of polymers, which will reduce their conductivities and electrical activities further [22]. The products prepared by electrodeposition method have the highest specific capacitance (SC), but huge investment is needed. The electrostatic interaction assembly always involves complicated processing-steps. By contrast, the chemical co-precipitation is the simplest method. However, it was noted that the co-precipitation method might get difficulties in forming a uniform polymerization condition on the micro-level and this synthesis was indisciplinable. Thus, it is essential to exploit a convenient, cost-effective and controllable synthesis technology.

The inverse miniemulsion technique, i.e. the water-in-oil (W/O) miniemulsion, show potential to prepare composites with controlled sizes and special structures, which can be prepared with the same way to direct miniemulsion (O/W). A W/O miniemulsion contains a nonpolar continuous phase and a polar dispersed phase. The surfactants and emulsion devices are key factors to prepare the W/O miniemulsion. The surfactants can be adsorbed onto the interface of water and oil, which will prevent droplets growth or coalescence. As miniemulsion is a kinetic equilibrium system, the energy input from emulsion devices is required to maintain the dispersed phase droplets within nano scales [23]. Although emulsion devices such as rotor-stators, high pressure homogenizers, and ultrasonic instrument can provide mechanical energy to form miniemulsion, ultrasonic instrument is the commonly applied emulsion device because of its efficiency at lab scale. Additionally, the cavitation bubbles produced by ultrasonic waves are most likely a secondary effect, then the collapse of the bubbles can prevent or retard the coalescence of the monomer droplets [24]. Thus, the diffusion of monomer is restrained and the polymerization occurs in the singular droplets, which are benefit to form the homogeneous particle size. By comparison, the droplets size of W/O miniemulsion is smaller and the stabilization time of miniemulsion is longer than O/W miniemulsion. Based on the properties of miniemulsion, the method can be used to synthesize a series of hybrid nanomaterials, nanogels and nanocapsules [25-28]. However, only a few papers have reported synthesis of electrode materials for supercapacitors by the miniemulsion method. For example, Yu et al. [29] synthesized nanowires and nanobelts brinessite-type MnO_2 by microwave-assisted emulsion process, revealing that the nano-MnO_2 structures exhibited a SC of 227 F g^{-1} at the c.d. of 0.2 mA cm^{-2}. Zhang et al. [30] fabricated the

layered PPyGO-SDBS composites in situ emulsion polymerization, which had outstanding property as electrode materials of supercapacitors. The SC went up to 483 F g^{-1} at a c.d. of 0.2 A g^{-1}, but the SC only retained 80% after 1000 cycles. In our preliminary work, we prepared MnO_2/PPy composites by O/W miniemulsion and only discussed the influence of molar ratio (Py/$KMnO_4$) on their electrochemical properties [31]. Additionally, MnO_2/PPy in O/W system had a poor compatibility with the PVDF, which might cause the low stability of composite materials.

In this study, the main focus of the exploration is to prepare the stable miniemulsion and synthesize MnO_2/PPy composites using facile W/O miniemulsion technology. The effects of HLB, $KMnO_4$ amount and reaction time on the electrochemical properties of MnO_2/PPy composites were studied in detail. The MnO_2/PPy composites have been proved to exhibit better performance than those of individual components, so the preparation process of pure MnO_2 or PPy were omitted to condense the content. It was revealed that the products prepared by this novel method showed well electrochemical properties and stability as electrode material for supercapacitors.

2. EXPERIMENTAL

2.1 Materials and reagents

All of the chemicals used are of analytical grade. Pyrrole (Py) (Macklin Biochemical Co., Shanghai, China) was firstly purified with decompression. Then the distilled Py was stored below 4 °C and set aside. Potassium permanganate ($KMnO_4$) was grinded carefully before used. Cyclohexane (C_6H_{12}), and anhydrous ethanol were supplied by Tianjin Guangfu Fine Chemical Research Institute, and applied as received in this work. Span 80 (Sorbitan monooleate) and Tween 80 (Polyoxyethylene sorbitan monooleate) were purchased from Tianjin Beichen Fangzheng Reagent Factory. Deionized water was produced by a GWA-UN to Pure & Ultrapure water treatment system (Purkinje General).

2.2 Preparation of W/O miniemulsion

The experimental procedure was illustrated in Figure 1. The W/O miniemulsion was prepared using cyclohexane and water with the aid of surfactants, including three key steps: (1) the oil phase was prepared by dissolving Span 80 (HLB=4.3) in cyclohexane, while the water phase was prepared by mixing deionized water and Tween 80 (HLB=15); (2) The water phase was added into the oil phase drop by drop with stirring for 15 min to obtain a coarse emulsion, the mass ratio of oil phase to water phase was 10:1; (3) The coarse emulsion was homogenized by ultrasonic (Scientz-IID, 475 W, amplitude 40%) for 5 min in an ice-bath to prepare the W/O miniemulsion.
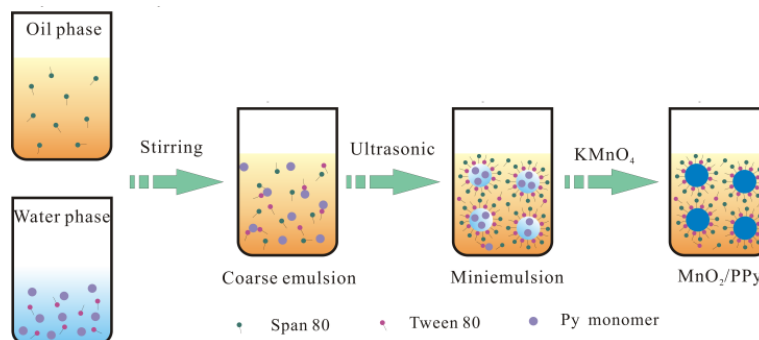
Figure 1. Schematic illustration of the synthesis of MnO_2/PPy composites by W/O miniemulsion.

2.3 Preparation of MnO$_2$/PPy composites

The monomer miniemulsion was obtained as the above steps (1)-(3). What different was that the water phase (10 g) consisted of deionized water, Tween 80 and Py monomer. Subsequently, a certain amount of $KMnO_4$ was added to the monomer miniemulsion with intensely agitating for 2 h. Finally, the precipitates collected from the centrifuge were further washed by cyclohexane, anhydrous ethanol and deionized water thoroughly to remove the surfactants and some impurities, then dried for 12 h at 75 °C to obtain MnO_2/PPy composites.

2.4 Characterization

The droplets size of miniemulsion was measured via dynamic light scattering (DLS, Zetasizer Nano-ZS90, Malvern Instruments, UK). Droplets dimension was recorded immediately after ultrasonic by diluting the sample with the oil phase. The stability of miniemulsion was an evaluation criterion for miniemulsion. Herein, the stabilization time, i.e. transfer the prepared miniemulsion to 25 mL cylinders with stoppers, aging at room temperature until observe the separation between water phase and oil phase, was applied to test the stability of miniemulsion. The bonding properties of MnO_2/PPy composites were analyzed through Fourier transform infrared spectroscopy (FTIR, Spectrum Two). The crystal form was verified via X-ray diffraction (XRD, DX-2700) with a scanning rate of 5° min^{-1} and the 2θ of 10° to 80° under Cu $K\alpha$ radiation. The morphologies were determined by a high resolution transmission electron microscope (HRTEM, JEM-2100F). The thermal stability was investigated by thermogravimetric analyzer (TGA, STA-449-F3) with pure N_2 gas from 50 to 1000 °C by employing a heating speed of 10 °C min^{-1}.

2.5 Electrochemical tests

All tests were carried out at ambient temperature. Electrochemical tests were completed in a three-electrode system by a CHI 660E workstation (Chenhua, Shanghai) at 0-0.8 V in 0.5 mol L^{-1} $NaSO_4$ electrolyte. Platinum and a standard Hg/Hg_2Cl_2 served as the auxiliary electrode and the reference electrode, respectively. The manufacturing process of working electrodes as follows: firstly,

70 wt % active materials, 20 wt % acetylene black and 10 wt % PVDF were blended. Then the mixture was dispersed in an NMP to produce a uniform paste; secondly, the paste was spread onto a 1×1 cm^2 porous nickel, then treated at 60 °C for 4 h to evaporate the NMP; lastly, the sheet were pressed below 10 MPa for 10 min. EIS was performed at the frequency between 0.01 Hz and 100 kHz under voltage amplitude of 5 mV. The effective mass of electrode ranged from 0.5-1.0 mg cm^{-2}.

3. RESULTS AND DISCUSSION

3.1 Stability of W/O miniemulsion
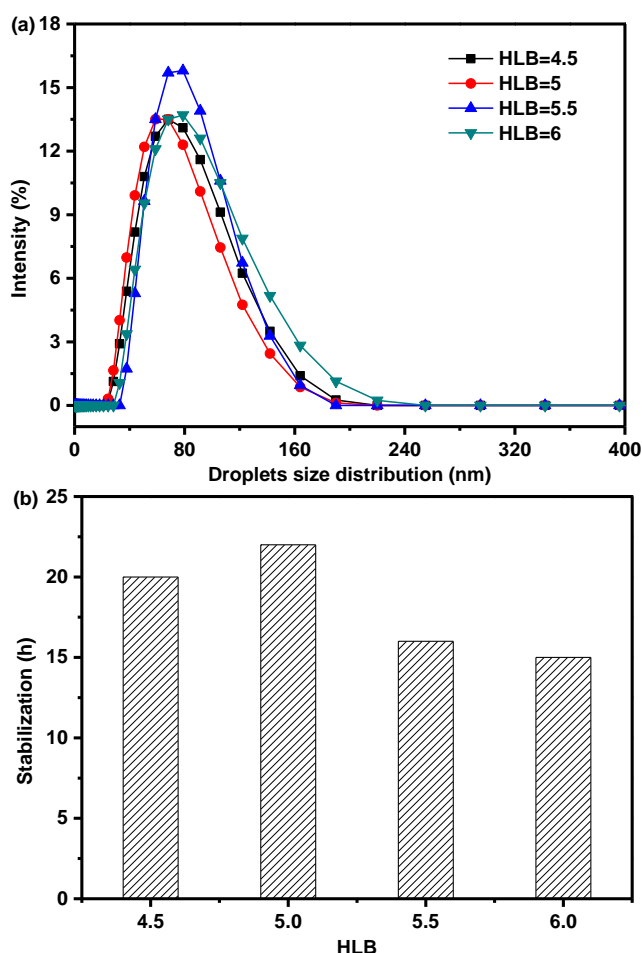
Figure 2. (a) The droplets size distribution and (b) stabilization time of miniemulsion.

The HLB, one of the most widely used indicators of the surfactant for a given application, is a measure of a surfactant tendency to oil or water phase. In this study, Span 80 and Tween 80 were chosen as the hydrophilic and lipophilic surfactant, respectively. The HLB of the mixed surfactant system (HLB$_{mix}$) is calculated by the following equation [32]:

$$HLB_{mix} = HLB_A \times q_A + HLB_B \times q_B \qquad (1)$$

where HLB_A, HLB_B, q_A and q_B are the HLB value and the mass fractions of Span 80 and Tween 80, respectively. For the W/O miniemulsion, the required HLB ranged from 3 to 6.

Figure 2a illustrates the effect of HLB on the droplets size distribution of the miniemulsion. It can be clearly seen that the droplets size of the miniemulsion decreases as HLB increase, and then increases as the HLB further increase. By contrast, when the HLB is 5, the droplets size distribution and average droplets size (58 nm) are smallest. Figure 2b displays the influence of HLB on the stabilization time of the miniemulsion. It indicates that the longest stabilization time of miniemulsion is about 22 h at HLB=5, and the stabilization time decreases with HLB further increased. These results show that the hydrophilic-lipophilic is tend to balance at HLB=5. Without the optimal HLB, the balance between hydrophilic and lipophilic will be disrupted, thus the droplets size and stabilization time are changed. Nejadmansouri et al. [33] researched the effect of HLB on physicochemical properties and stability of fish oil miniemulsions. The results showed that a reduction in particle size was found as improving the HLB from 9 to 12. Then its dimension kept relatively constant at higher HLB. It reveals the fact that each emulsion system owns an optimal HLB value. Therefore, the HLB of 5 is selected to ensure the stability of the miniemulsion system for preparation of MnO_2/PPy composites.

3.2 Structure and morphology of MnO_2/PPy composites
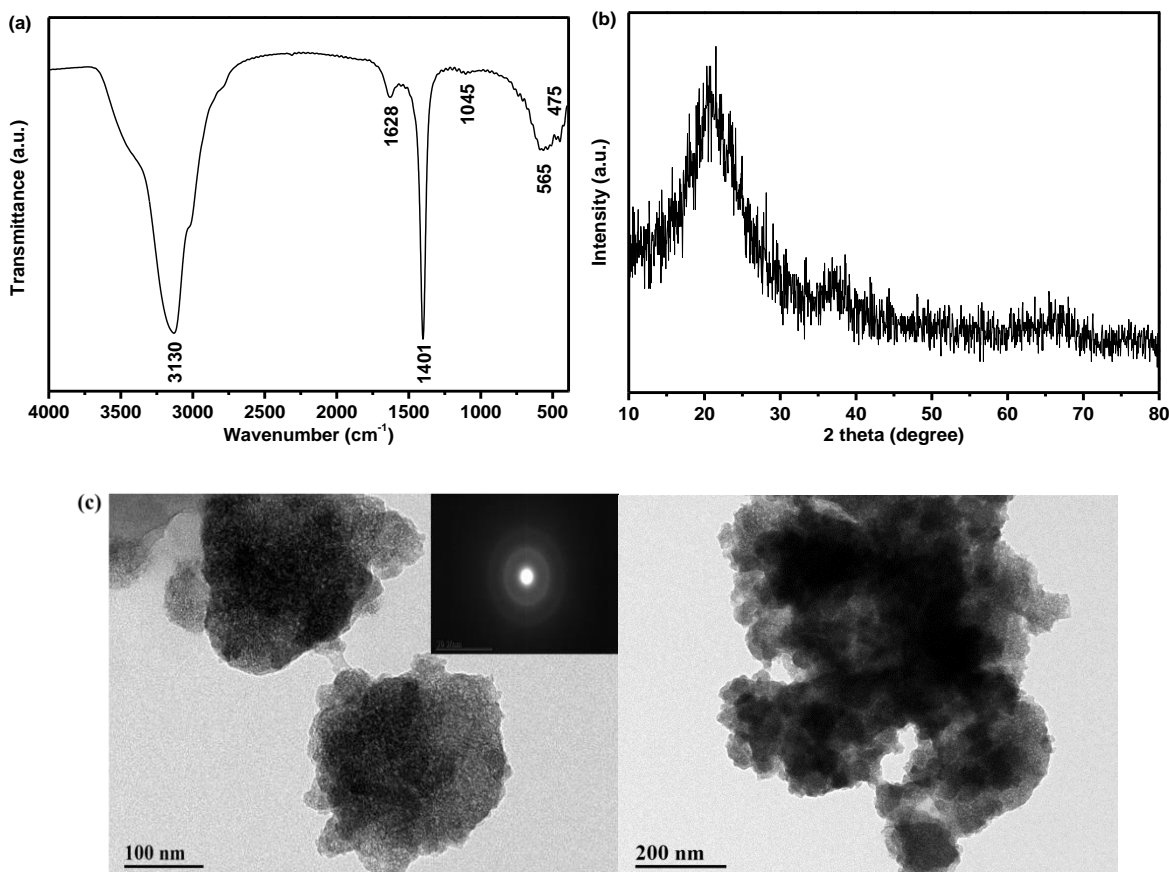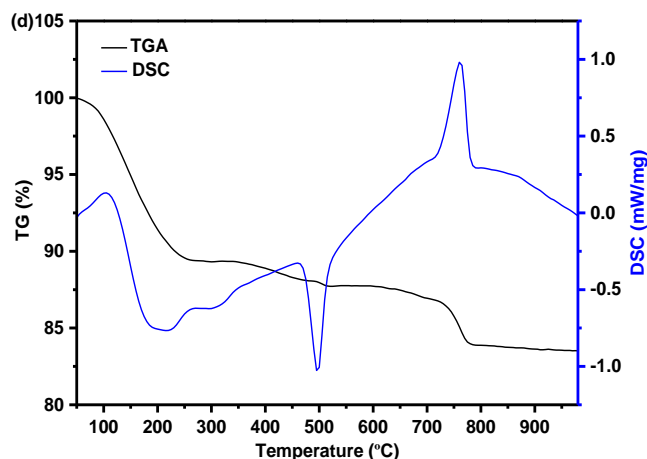
Figure 3. (a) FTIR spectra, (b) XRD patterns, (c) HRTEM image (the *inset* is the corresponding SEAD pattern), and (d) TGA curve with DSC curve of MnO_2/PPy composites.

The structure and composition of MnO_2/PPy composites were characterized through the FTIR. As seen in Figure 3a, the absorption peaks appear at about 565 and 475 cm^{-1} belong to the Mn-O stretching vibrations of $[MnO_6]$ octahedral in α-MnO_2 [34]. The main characteristic peaks of PPy in MnO_2/PPy composites are assigned as follows. The peak at 1628 cm^{-1} is assigned to the stretching vibration of the PPy ring. The bands at 1401 cm^{-1} and 1045 cm^{-1} are attributed to the in-plane deformation of the C-H and N-H, respectively [15, 34]. The peak at approximately 3130 cm^{-1} is ascribed to the stretching vibration of -OH groups of the samples. These results suggest that the MnO_2/PPy composites are prepared via the W/O miniemulsion technology successfully.

Figure 3b shows the XRD pattern of MnO_2/PPy composites. The broad bands from 15° to 30° are the characteristic peaks of amorphous PPy. The crest of $2\theta = 23°$ is characteristic of amorphous PPy, resulting from the repeat unit of pyrrole ring. Both broad peaks at $2\theta = 37.1°$ and 66.7° (JCPDS 44-014) indexed to the phase of α-MnO_2 [4]. The results are coincided to the report of Gan et al. [35]. The reason may be that a part of the MnO_2 transformed from crystalline state into amorphous form during the redox polymeration. On the other hand, MnO_2 can oxidize the pyrrole monomer [36], and thus the amount of MnO_2 reduced in the system. Therefore, the intensity of MnO_2 is weak, which is in line with the result of the FTIR tests.

Figure 3c exhibits the HRTEM photograph of MnO_2/PPy composites. Apparently, the MnO_2/PPy composites consist of a larger dimension of quasi-spherical particles and the diameter is ~200 nm. The particle size is much bigger than the miniemulsion droplets and the surface becomes irregular and coarse. This could be due to miniemulsion droplets or nancomposites crosslink during the redox reaction. As shown in the corresponding selected area electron diffraction (SAED) pattern, there are no bright spots exist, indicating that the MnO_2/PPy composites are amorphous, which agrees with the results of the XRD.

Figure 3d shows the TGA curve and the corresponding differential scanning calorimetric (DSC) curve of MnO_2/PPy composites. The first mass loss starts from 94 °C, which is associated with concurrent removal of water and carbon dioxide. The second mass loss is the PPy skelecton decomposition at a temperature ranging from 300 to 600 °C, the interval is separated into two regions

at ~505 °C in the TGA curve, and it fits well with the exothermic peak in DSC curve. On the basis of this fact, it is believed that the decomposition process of PPy is open the carbon chains at first, and then decomposition further. The third mass loss after 600 °C associated with the evolution of MnO_2 to Mn_2O_3 accompanied by the loss of oxygen, and residual percentage of MnO_2/PPy is 83.49%, which is much higher than the report by Yao et al. and Ji et al. [37-39]. The TGA results associated with the DSC curve indicate that MnO_2/PPy composites are highly stable, and the synergistic interaction between MnO_2 and PPy chains play an important role.

3.3 Electrochemical properties

3.3.1 Effect of HLB
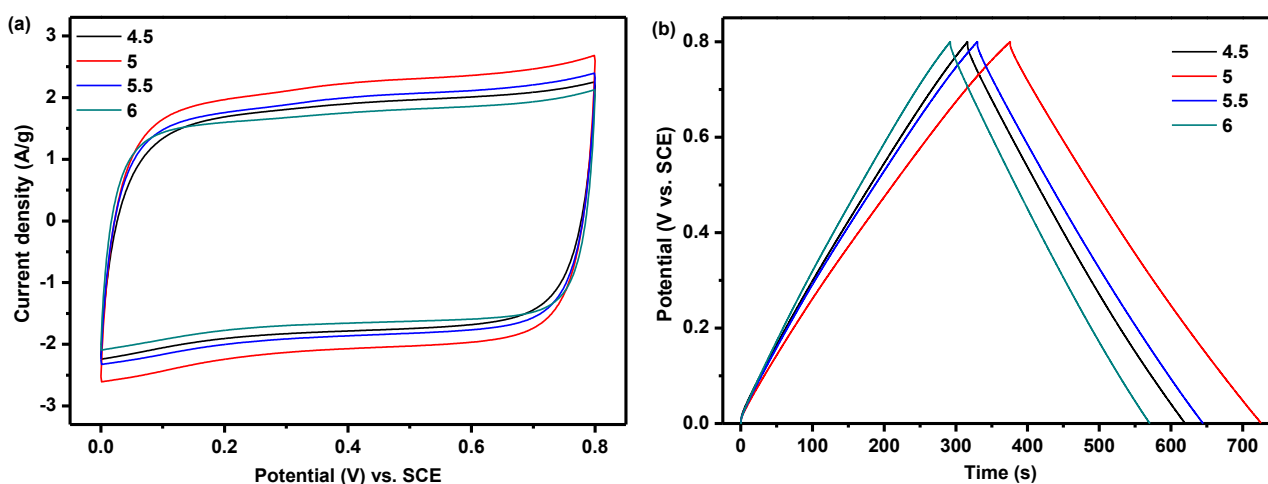
Figure 4. Effect of HLB on MnO_2/PPy electrodes: (a) CV at a scan rate of 10 mV s^{-1}, and (b) GCD at a c.d. of 0.5 A g^{-1}.

Figure 4 displays the influence of HLB on the electrochemical properties of MnO_2/PPy electrodes. The figure reveals that the HLB significantly affects the electrochemical performances. As expected, the trend of CV and GCD curves of MnO_2/PPy electrodes is match well with each other. All CV are of the typical rectangular shape (Figure 4a), indicating the the fast and reversible redox reactions of the sample. The voltammogram shape is close to that of the electrical double layer materials [40]. The SC increases with an increase of HLB at first until the optimal HLB of 5 is met, and then reduces with further increase of the HLB. The SC of MnO_2/PPy electrodes is estimated by the discharging time based on the following formula:

$$C = \frac{I \cdot \Delta t}{m \cdot \Delta V} \qquad (2)$$

where C (F g^{-1}) is the SC, I (A) is the discharging current, Δt (s) is the discharging time, m (g) is the mass of active materials, and ΔV (V) is the voltage window.

As seen in the Figure 4b, the typical triangle indicates superior reversibility of charge/discharge reactions of the composite electrodes. The SCs of MnO_2/PPy electrodes are 189.4, 218.7, 196.9 and 174.0 F g^{-1} at HLB of 4.5, 5, 5.5 and 6, respectively. This may be due to the fact that a miniemulsion

system corresponds to an optimal HLB, and the HLB value of compound surfactants is obtained by adjusting the ratio of hydrophilic to lipophilic surfactant. At the optimal HLB, the surfactant covers the surface of droplets to prevent the droplet coalescing. However, the balance of hydrophilic-lipophilic and the stability of droplets will be destroyed when the HLB deviates, further impacting the electrochemical properties. Gullapalli et al. [41] also determined that the HLB was a critical factor for miniemulsion.

3.3.2 Effect of $KMnO_4$ amount
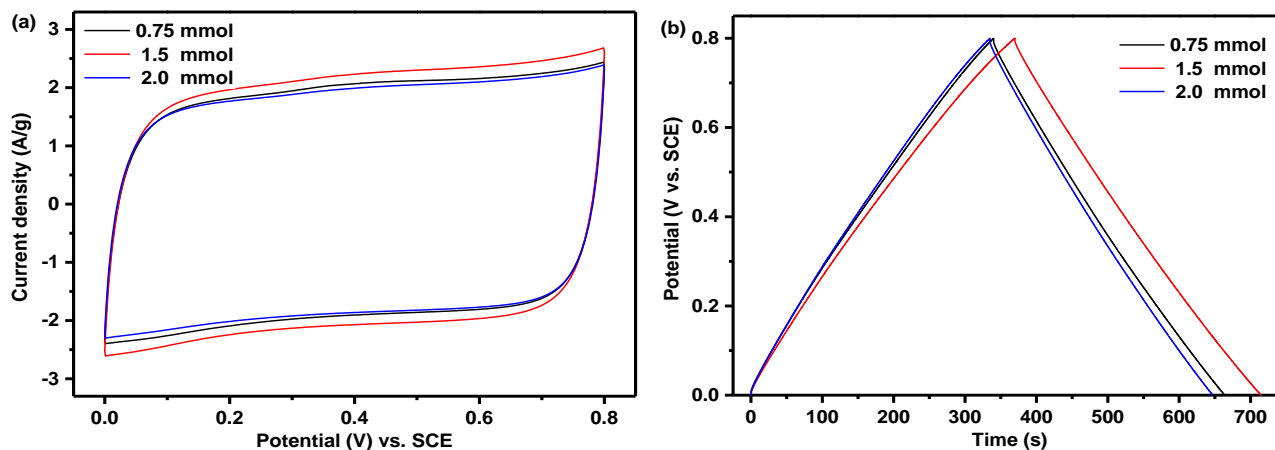
Figure 5. Effect of $KMnO_4$ amount on MnO_2/PPy electrodes: (a) CV at a scan rate of 10 mV s^{-1} and (b) GCD at a c.d. of 0.5 A g^{-1}.

When the HLB and the reaction time keep at 5 and 2 h, the effect of $KMnO_4$ amount on electrochemical properties of MnO_2/PPy samples were measured by three-electrode cell system. Figure 5 gives the CV and GCD of the MnO_2/PPy electrodes in different $KMnO_4$ amount at the scan rate of 10 mV s^{-1} in the Na_2SO_4 aqueous (0.5 mol L^{-1}). The current area shows an increasing trend at first and subsequently decreases when the $KMnO_4$ is increased from 0.75 to 2.0 mmol. The current area reaches the biggest value when $KMnO_4$ is 1.5 mmol. As indicated in Figure 5b, the highest capacitance is 215.6 F g^{-1} at 1.5 mmol of $KMnO_4$. The trend is in accordance with the CV results. This attributes to partial Py monomers are oxidized at a low quantity of $KMnO_4$ in the system. On the other hand, the structure of PPy will be damaged during the reaction between PPy and a high quantity of $KMnO_4$. This destruction is caused by the strong oxidation ability of $KMnO_4$ [39]. In addition, the solubility of $KMnO_4$ is 6.4 g per 100 mL water at 20 °C, which limits the usage amount of $KMnO_4$. Accordingly, the 1.5 mmol of $KMnO_4$ is recommended.

3.3.3 Effect of reaction time

The influence of reaction time on the electrochemical performances of MnO_2/PPy electrodes was evaluated by regulating the reaction time from 1.5 to 3 h, when the HLB and $KMnO_4$ were 5 and 1.5 mmol, respectively. As shown in Figure 6, such a variation trend of the reaction time is similar to

the effects of the HLB and $KMnO_4$. Obviously, the maximum current area and SC were achieved at 2 h. The SCs of the electrodes can be evaluated according to Eq. (2), and the SCs are 226.2, 288.7, and 208.1 F g^{-1} when the reaction times are 1.5, 2 and 3 h, respectively. The reason for this variation could be that redox reaction between $KMnO_4$ and Py was not completely within 1.5 h, while Py would be overoxided beyond 2 h. Thus, 2 h is the favored reaction time for the synthesis of MnO_2/PPy composites with excellent capacitive properties.
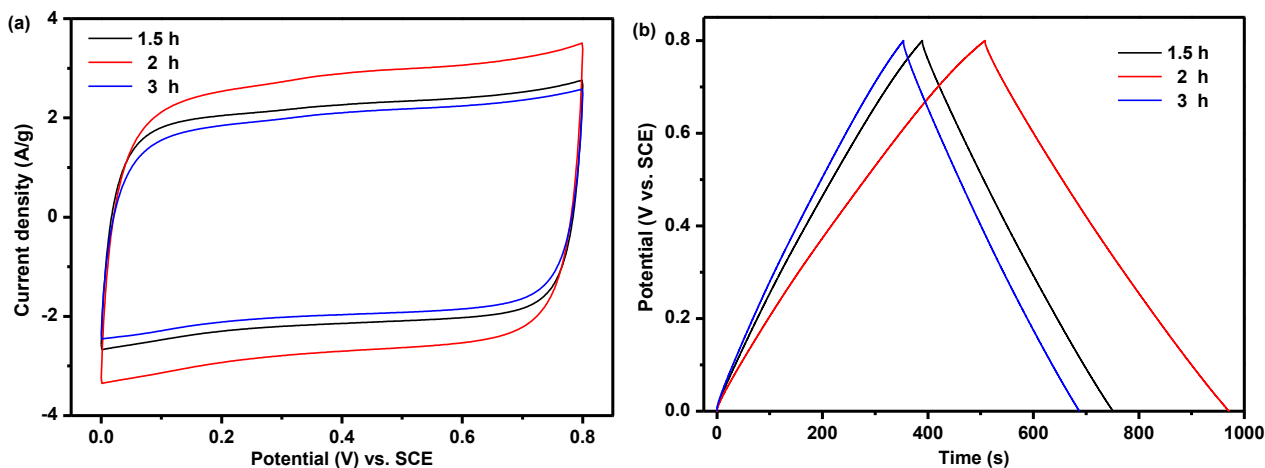
Figure 6. Effect of reaction time on MnO_2/PPy electrodes: (a) CV at a scan rate of 10 mV s^{-1} and (b) GCD at a c.d. of 0.5 A g^{-1}.

The above experimental results suggest that the appropriate preparing condition can be realized at the HLB of 5, $KMnO_4$ of 1.5 mmol and reaction time of 2 h. Under this condition, the electrochemical performance of as-synthesized MnO_2/PPy nanoparticles were investigated systematically by CV, GCD, EIS and cycling life tests at room temperature. In Figure 7a, the CVs were studied at various scan rates for MnO_2/PPy composites. It was found that the current area rises with an increase of the scan rate. These curves are apparent difference from the rectangle at a high scan rate (100 mV s^{-1}), indicating that the high scan rate directly reduce the diffusion of Na^+ into the active material. MnO_2/PPy in the neutral Na_2SO_4 aqueous is primarily controlled by the inserting/removing Na^+ from the electrolyte into the nanocomposite or from the composites into the electrolyte [19, 34]. The Na^+ ions derived from the electrolyte can readily diffuse into the active sites of the electrodes at a low scan rate. This diffusion results in a complete insertion process. At a high scan rate, the diffusion time was decreased for the Na^+ ions to pass into the inner surface of the electrode. Moreover, the valid interaction between the ions and the active material was extremely decreased [2, 42]. Therefore, the active material in the interior surface gives little contribution to the SC, leading to an obvious difference from the ideal rectangle of the CV.

The GCD tests were performed in 0.5 mol L^{-1} Na_2SO_4 electrolyte at different current densities from 0-0.8 V (Figure 7b). The charging time is close to the discharging time, implying high reversibility and efficiency of the active material, either. The PPy/MnO_2 electrode at different current densities displays that SC drops from 288.7 to 157.5 F g^{-1}. One possible reason of this decrease in SC is similar with the explanation of CV. Moreover, the hydrated cation diffusion resistance in the bulk

electrolyte results in a great ohmic potential drop at a high c.d. and thus leads to the fast reduction of the SC.
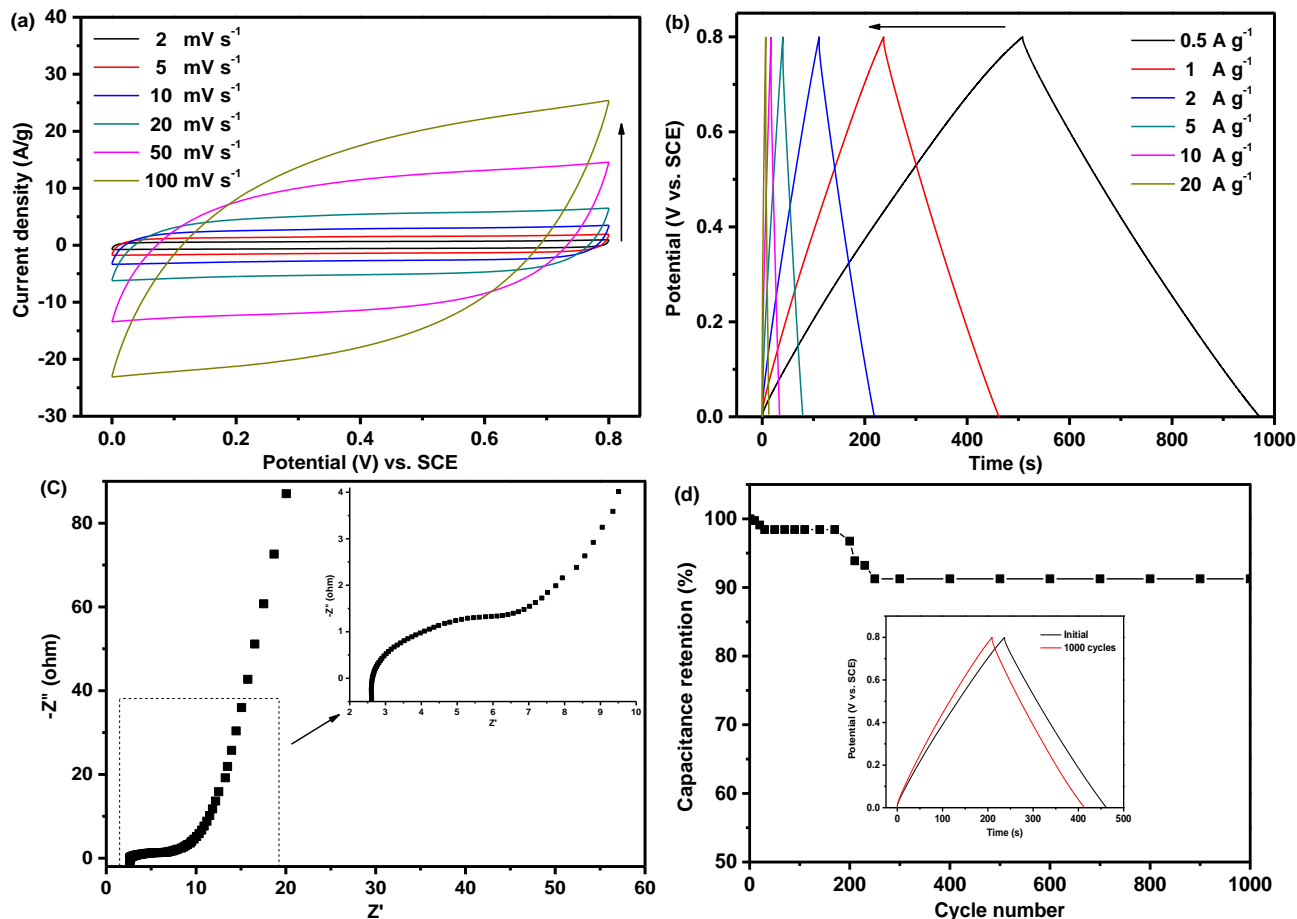
Figure 7. (a) CV, (b) GCD, (c) EIS test and (d) cycle life test of MnO_2/PPy electrodes at 1 A g^{-1} for 1000 times.

The electrochemical impedance spectroscopy (EIS) was employed as a measurement for the electrochemical characterization of the electrodes. In Figure 7c, the Nyquist plot contains a semicircle portion and a linear portion. At a high frequency, the semicircle diameter relates to the electron transfer resistance (R_{ct}=3.9 Ω). In addition, the internal resistance (R_s=2.6 Ω) of the active materials can be observed from the high frequency intercept of the horizontal axis. The Rs includes the intrinsic resistance of the active material, the contact resistance at the interface active material/current collector and the resistance of the electrolyte [43]. At a low frequency, the linear part tends to a vertical line corresponds to the pseudo-capacitance and well ions diffusion process. The observation implied that the decreased R_{ct} and R_s were confident to improve the pseudo-capacitive properties of the PPy/MnO_2 electrodes.

As we all known, the cycling life of the electrode is an important issue for supercapacitors. Figure 7d shows the cycle performance of PPy/MnO_2 materials at a c.d. of 1 A g^{-1} by GCD tests. It is clear that a significant decline of the SC is occur at 250 cycles, indicating that much more unstable MnO_2 and PPy dissolve and/or detach in the electrolyte solution [44]. After that, the capacitance retention of PPy/MnO_2 electrode is maintained at 91.3%. The charge and discharge lines of the inset (Figure 7d)

for the first and last cycles are displayed for comparison. Notably that the triangular shape of the charge/discharge curve remains symmetric after 1000 cycles. This might be ascribed to cooperativity between PPy and MnO_2. PPy can improve the conductivity of the complex material and keep the MnO_2 from diffusing into the electrolyte at a certain extend. In turn, the MnO_2 in composites could make the PPy chains steady by rigid support during the redox reaction. A comparison of the electrochemical performance of the PPy/MnO_2 electrodes with that of similar electrodes in literature is listed in Table 1. The electrochemical properties of PPy/MnO_2 are as well as most of the same composite materials. Hence, W/O miniemulsion may be a promising candidate method for preparing PPy/MnO_2 composites.

Table 1. Comparison of the electrochemical properties of the PPy/MnO_2 electrodes

Electrode materials	Synthetic method	Current density (or scan rate)	Specific capacitance (F g^{-1})	Capacitance retention	Ref.
MnO_2/PPy thin film	Electrochemical co-deposition	2 mA cm^{-2}	~180 (double-electrode system)	90% (1000 cycles)	[3]
PPy/γ-MnO_2	Electrodeposition	2 mA cm^{-2}	141.6 (double-electrode system)	50% (500 cycles)	[19]
Nanotube PPy/MnO_2	PPy nanotubes as template	2 A g^{-1}	276 (three-electrode system)	88.6% (800 cycles)	[39]
PPy/MnO_2/ PPF films	Chemical oxidation polymerization	2 A g^{-1}	110 (double-electrode system)	94% (1500 cycles)	[42]
MnO_2/PPy	Chemical oxidative polymerization	0.1 A g^{-1}	~182 (three-electrode system)	96.5% (400 cycles)	[45]
β-MnO_2/PPy nanorod	Chemical oxidative polymerization	1 A g^{-1}	294 (three-electrode system)	92.6% (1000 cycles)	[46]
MnO_2/PPy nanotubes	MnO_2 nanotubes as template	50 mV s^{-1}	233 (three-electrode system)	90% (1000 cycles)	[47]
MnO_2/PPy	W/O miniemulsion	0.5 A g^{-1}	288.7 (three-electrode system)	91.3% (1000 cycles)	This work

4. CONCLUSIONS

MnO$_2$/PPy composites have been first prepared by W/O miniemulsion successfully. The stable inverse miniemulsion was prepared and used to synthesize the MnO_2/PPy composites. The optimum conditions for preparing MnO_2/PPy composites were the HLB of 5, $KMnO_4$ of 1.5 mmol and reaction

time of 2 h. Under this case, the MnO_2/PPy composites exhibited high SC of 288.7 F g^{-1} at the c.d. of 0.5 A g^{-1}, and the SC can retain 91.3% after 1000 cycles at 1 A g^{-1}. It was proved that the synergistic effect of MnO_2 and PPy make contribute to enhance the electrochemical performances of MnO_2/PPy composites. As a result, the W/O miniemulsion approach provide an effective and governable route for the synthesis of MnO_2/PPy composites and other MnO_2-based composites.

References

1. P. Simon and Y. Gogotsi, *Nat. Mater.*, 7(2008) 845.
2. P. K. Nayak and N. Munichandraiah, *Micropor. Mesopor. Mat.*, 143(2011) 206.
3. R. K. Sharma, A. C. Rastogi and S. B. Desu, *Electrochim. Acta*, 53(2008) 7690.
4. J. Wang, Y. Yang, Z. Huang, F. Kang, *Electrochim. Acta*, 130(2014) 642.
5. W. Ni, D. Wang, Z. Huang, J. Zhao and G. Cui, *Mater. Chem. Phys.*, 124(2010) 1151.
6. L. J. Han, P. Y. Tang and L. Zhang, *Nano Energy*, 7(2014) 42.
7. J. Li, T. L. Que and J. B. Huang, *Mater. Res. Bull.*, 48(2013) 747.
8. S. Liu, H. F. Dong, J. P. Du, X. J. Qin and G. J. Shao, *Ionics*, 20(2014) 295.
9. H. Zhou, Z. Yan, X. Yang, J. Lv, L. Kang and Z. H. Liu, *Mater. Chem. Phys.*, 177(2016) 40.
10. F. Grote and Y. Lei, *Nano Energy*, 10 (2014) 63.
11. H. Farrokhi, O. Khani, F. Nemati and M. Jazirehpour, *Synth. Met.*, 215(2016) 142.
12. J. S. Lee, D. H. Shin and J. Jang, *Energ. Environ. Sci.*, 8(2015) 3030.
13. S. Yang, P. Yan, Y. Li, K. Ye, K. Cheng, D. Cao, G. Wang and Q. Li, *Electrochim. Acta*, 182(2015) 1153.
14. J. Joo, J. K. Lee, S. Y. Yee, K. S. Jang, E. J. Oh and A. J. Epstein, *Macromolecules*, 33(2000) 5131.
15. J. Li, L. Cui and X. G. Zhang, *Appl. Surf. Sci.*, 256(2010) 4339.
16. J. Zhang, Y. Shi, Y. Ding, W. Zhang and G. Yu, *Nano Lett.*, 16(2016) 7276.
17. X. Duan, J. Deng, X. Wang, J. Guo and P. Liu, *Electrochim. Acta*, 210(2016) 646.
18. K. Q. Ding and F. M. Cheng, *Synth. Met.*, 159(2009) 2122.
19. A. Bahloul, B. Nessark, E. Briot, H. Groult, A. Mauger, K. Zaghib and C. M. Julien, *J. Power Sources*, 240(2013) 267.
20. W. Ma, Q. Shi, H. Nan, Q. Hu, X. Zheng, B. Geng and X. Zhang, *RSC Adv.*, 5(2015) 39864.
21. J. F. Zang and X. D. Li, *J. Mater. Chem.*, 21(2011) 10965.
22. J. G. Wang, F. Y. Kang and B. Q. Wei, *Prog. Mater. Sci.*, 74(2015) 51.
23. J. M. Asua, *Prog. Polym. Sci.*, 39(2014) 1797.
24. F. G. Donnan, Technical Aspects of Emulsion, (1935) A. Harvey, London.
25. K. Landfester, *Angew Chem. Int. Ed.*, 48(2009) 4488.
26. J. K. Oh, C. B. Tang, H. F Gao, N. V. Tsarevsky and K. Matyjaszewski, *J. Am. Chem. Soc.*, 128(2006) 5578.
27. K. Landfester and V. Mailänder, *Expert Opin. Drug Del.*, 10(2013) 593.
28. Z. Cao and U. Ziener, *Nanoscale*, 5(2013) 10093.
29. P. Yu, X. Zhang, Y. Chen, Y. Ma and Z. Qi, *Mater. Chem. Phys.*, 118(2009) 303.
30. Y. Zhang, M. Li, L. Yang, K. Yi, Z. Li and J. Yao, *J. Solid State Electrochem.*, 18(2014) 2139.

31. F. Liang, Z. Liu, Y. Liu, *J. Mater. Sci.: Mater. Electron.*, 28(2017) 10603.
32. L. Wang, J. Dong, J. Chen, J. Eastoe and X. Li, *J. Colloid Interface Sci.*, 330(2009) 443.
33. M. Nejadmansouri, S. M. H. Hosseini, M. Niakosari, G. H. Yousefi and M. T. Golmakani, *Colloids and Surfaces A: Physicochem Eng. Aspects.*, 506(2016) 821.
34. J. G. Wang, Y. Yang, Z. H. Huang and F. Kang, *Elctrochim. Acta*, 130(2014) 642.
35. J. K. Gan, Y. S Lim, N. M. Huang and H. N. Lim, *Appl. Surf. Sci.*, 357(2015) 479.
36. O. Khani, F. Nemati, H. Farrokhi and M. Jazirehpour, *Synth. Met.*, 220(2016) 567.
37. Q. Lu and Y. Zhou, *J. Power Sources*, 196(2011) 4088.
38. W. Yao, H. Zhou and Y. Lu, *J. Power Sources*, 241(2013) 359.
39. J. Y. Ji, X. Y. Zhang, J. Y. Liu, L. Peng, C. Chen, Z. Huang, L. Li, X. Yu and S. Shang, *Mater. Sci. Eng. B*, 198(2015) 51.
40. P. Simon and Y. Gogotsi, *Nat. mater.*, 7(2008) 845.
41. R. P. Gullapalli and B. B. Sheth, *Eur. J. Pharm. Biopharm.*, 48(1999) 233.
42. M. Jin, G. Han, Y. Chang, H. Zhao and H. Y. Zhang, *Electrochim. Acta*, 56(2011) 9838.
43. R. Poonguzhali, N. Shanmugam, R. Gobi, A. Senthilkumar and G. Viruthagiri, *J. Power Sources*, 293(2015) 790.
44. P. Soudan, J. Gaudet, D. Guay, D. Bélanger and R. Schulz, *Chem. Mater.*, 14(2002) 1210.
45. L. Yuan, C. Wan and L. Zhao, *Int. J. Electrochem. Sci.*, 10 (2015) 9456.
46. J. Zang and X. Li, *J. Mater. Chem.*, 21(2011) 10965.
47. W. Yao, H. Zhou and Y. Lu, *J. Power Sources*, 241(2013) 359.